Nanoscale

Accepted Manuscript

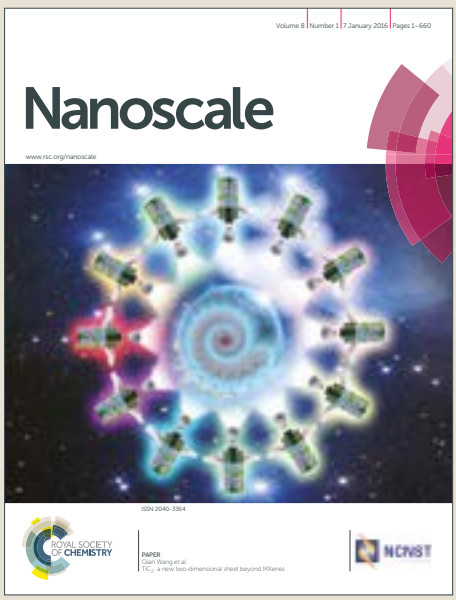

ROYAL SOCIETY OF CHEMISTRY

rsc.li/nanoscale

Revealing the nature of low-temperature photoluminescence peaks by laser treatment in Van der Waals epitaxially grown WS_2 monolayers

View Article Online
DOI: 10.1039/C8NR00719E

V. Orsi Gordo,[1,2] M. A. G. Balanta,[1,3] Y. Galvão Gobato,[1,*] F. S. Covre,[1] H. V. A. Galeti,[4] F. Iikawa,[2] O. D. D. Couto Jr.,[2] F. Qu,[5] M. Henini,[6,7] D. W. Hewak,[8] and C. C. Huang[8,†]

[1] *Departamento de Física, Universidade Federal de São Carlos, 13565-905, São Carlos, SP, Brazil*

[2] *Instituto de Física "Gleb Wataghin", Universidade Estadual de Campinas, 13083-859, Campinas, São Paulo, Brazil*

[3] *Universidade Federal de Uberlândia-FACIP, 38304-402, Ituiutaba, MG, Brazil*

[4] *Departamento de Engenharia Elétrica, Universidade Federal de São Carlos, 13565-905, São Carlos, SP, Brazil*

[5] *Instituto de Física, Universidade de Brasília, Brasília-DF 70919-970, Brazil.*

[6] *School of Physics and Astronomy, University of Nottingham, Nottingham NG7 2RD, UK*

[7] *UNESCO-UNISA Africa Chair in Nanosciences/Nanotechnology Laboratories, College of Graduate Studies, University of South Africa (UNISA), Muckleneuk Ridge, P O Box 392, Pretoria, South Africa*

[8] *Optoelectronics Research Centre, University of Southampton, Southampton, SO17 1BJ, UK*

(Dated: January 24, 2018)

Monolayers of transition metal dichalcogenides (TMD) are promising materials for optoelectronics devices. However, one of the challenges is to fabricate large-scale growth of high quality TMD monolayers with the desired properties in order to expand their use in potential applications. Here, we demonstrate large-scale tungsten disulfide (WS_2) monolayers grown by Van der Waals Epitaxy (VdWE). We show that, in addition to the large structural uniformity and homogeneity of these samples, their optical properties are very sensitive to laser irradiation. We observe a time instability in the photoluminescence (PL) emission at low temperatures in the scale of seconds to minutes. Interestingly, this change of the PL spectra with time, which is due to laser induced carrier doping, is employed to successfully distinguish the emission of two negatively charged bright excitons. Furthermore, we also detect blinking sharp bound exciton emissions which are usually attractive for single photon sources. Our findings contribute to a deeper understanding of this complex carrier dynamics induced by laser irradiation which is very important for future optoelectronic devices based on large scale TMD monolayers.

I. INTRODUCTION

View Article Online
DOI: 10.1039/C8NR00719E

Two-dimensional (2D) transition metal dichalcogenides (TMDs) are very attractive materials which show spin-valley coupled physics and strong excitonic effects which can be exploited in the next generation of optoeletronics devices[1–8]. The large electron and hole effective masses arising from the atomic *d*-orbitals along with reduced dielectric screening in 2D systems leads to exceptionally strong excitonic interactions and correlations between the charge carriers[9]. Despite the intense investigation of these materials which has occurred over the last years, the detailed nature of emission bands of 2D semiconductor materials, particularly for WS_2 and WSe_2, is still being unveiled by recent studies[5,8,10–13]. While the photoluminescence (PL) spectra of TMD monolayers (MLs) like MoS_2 or $MoSe_2$ usually show two well-defined peaks associated with neutral excitons and trions, the spectra of WSe_2 and WS_2 MLs at lower temperatures are rather more complex[11]. Strong emission bands which are observed on the lower energy side of the trion emission in WSe_2 and WS_2 have been attributed to radiative recombination of biexcitons[14–18]. However, intra and intervalley negatively charged excitons recombination has been spectrally resolved in the same energy range of the spectrum[11,13,19,20]. The complexity to identify the origin of the peaks in these materials probed by PL spectroscopy is increased by the addition of recombination of localized-exciton complexes bound to defects/crystal imperfections/impurities[8,11,12] and by the possibility of brightening of dark excitons[10].

The spectra of TMD MLs can also be strongly affected by laser irradiation. Recent studies found that the laser exposure increases considerably the trion/exciton PL intensity ratio accompanied by a small PL redshift in MoS_2, $MoSe_2$ and WS_2 monolayers[21–23]. It was shown that high laser excitation powers can quench the neutral exciton emission in MoS_2 MLs[22]. For WS_2, it has been shown that laser irradiation can also reduce emission from the lowest energy band of the spectrum, the so called localized state (LS) band, which is usually attributed to localized/donor-acceptor recombination states[11,21]. These laser induced effects were interpreted as monolayer photo-doping which can originate from the substrate[22] or due to the reduction of surface adsorbents[21]. Laser induced doping seems to lead samples to cyclic processes since the exposure of the MLs to air at room temperature after laser doping at low temperature seems to recover the original PL spectrum[22]. However, they depend on the type of substrate, sample preparation method, temperature, ambient conditions and aging[21,22]. This may lead to important consequences on the optical and magneto-optical properties of future devices and in studies of TMD MLs under intense laser excitation, such like investigations of exciton polaritons and many body effects[8,24]. However, few detailed studies have been performed in order to understand deeply the optical changes

View Article Online
DOI: 10.1039/C8NR00719E

and instabilities, especially in the case of WS_2 and WSe_2 which, as mentioned, usually have higher density of spectral features.

In addition to the relatively broader excitonic bands, the PL spectra of WS_2 and WSe_2 MLs have also revealed sharp emission lines which can exhibit anti-bunching[25–28]. These peaks are usually related to the presence of localized impurity states[29–31]. In WSe_2, while the light emission centers at the edges of the flakes appeared to be robust on a long timescale, practically all of them showed clear fluctuation effects on a short timescale; jittering of emission lines of the order of the linewidth (on a millisecond timescale) and larger jumps of lines on a timescale of seconds or minutes[32]. For WS_2, the sharp peaks were usually observed in specific areas in grain boundaries in triangle crystals grown by chemical vapour deposition (CVD) and were attributed to bound excitons trapped by surface impurities. These PL peaks can suddenly disappear during the PL measurements[33]. For liquid exfoliated WS_2 nanosheets (lateral dimensions of 20 to 150 nm), individual sharp peaks at different energies showed time fluctuations of positions and intensities which were associated with randomly fluctuating electrostatic environment[7].

In this manuscript, we investigate the effects of laser irradiation on the stability of the emission lines in WS_2 monolayers grown for the first time by Van der Waals epitaxy (VdWE)[34] (details are described in the Methods section and Supplementary Information). In addition to the large structural uniformity and homogeneity of these VdWE-grown WS_2 ML samples, we show that light emission due to carrier recombination reveals time dependent instabilities. By employing macro- and micro (μ) PL measurements, we monitor the variation in time of the intensity and spectral position of the neutral exciton (X), negative trions (T_1 and T_2), bound-exciton (X_B), and localized state (LS) emissions. We show that the PL spectrum as a whole evolves significantly with time, showing the appearance of additional emission bands and disappearance of others. Sharp peaks with linewidths of ≈ 2 meV were also observed. They appear/disappear in a time scale of a few seconds. We attribute these instability effects to laser induced ML doping which, due to the relatively slow time scale compared to carrier recombination lifetimes leads to unstable emission behaviour. In particular, we use the optical instability effect to attribute the so-labelled T_2 emission to a second trion state instead of a biexciton (XX) state. We also show that the time scale of the instability depends on the laser power density and probing spot. For low excitation intensities and large probing spots, the timescale for changes is in the minutes range. For higher laser excitation intensities and smaller spots, the PL time evolution occurs in few seconds and a clear redshift is observed. Under these conditions, at low temperature, the spectra do not recover their original shape when the excitation intensity is

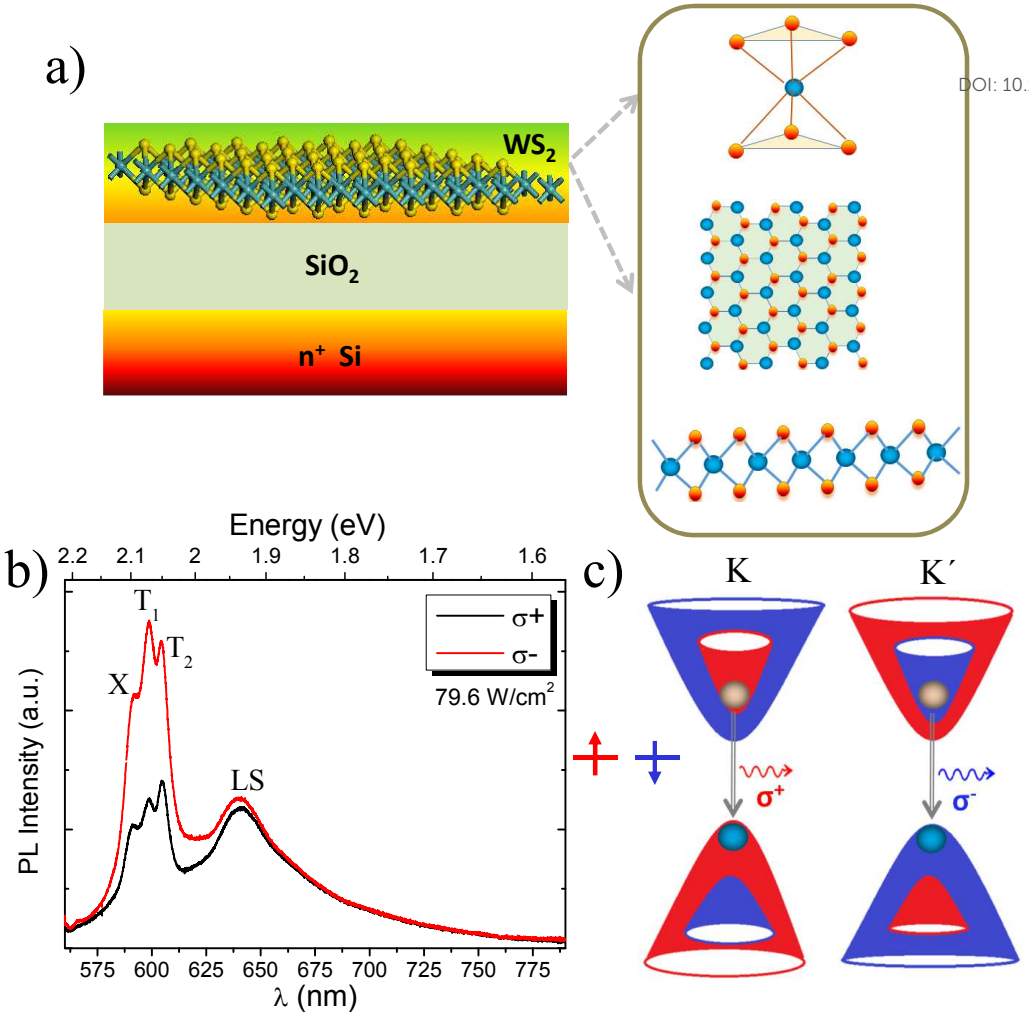

FIG. 1: (a) Illustration of monolayer WS_2 grown on SiO_2/Si substrate. Inset shows the coordination environment of W (blue sphere) in the crystal structure (upper panel), a side- (middle panel) and top- (lower) view of the monolayer WS_2 lattice. Sulphur is shown as golden spheres. (b) Circular polarization resolved PL measured on a WS_2 at 13 K and σ_- excitation. (c) Schematic diagram of valley-polarized light emitted by neutral exciton in K- (the left) and K'- (the right) valleys. The red (blue) color represents spin-up (down) states.

reduced to the low excitation regime. Moreover, for small probing areas, nonlinear increase in PL intensity with excitation power is observed. The time instability of WS_2 ML emission and its dependence on the probing spot size are particularly important for future devices of reduced dimensions, such as single photon sources based on TMDs.

II. RESULTS AND DISCUSSION

View Article Online
DOI: 10.1039/C8NR00719E

Figure 1(b) shows macro-PL spectra of the WS_2 monolayer measured at 13 K with laser power density of 79.6 W/cm^2. Excitation was σ_- circularly polarized and detection was performed for σ_+ (black curve) and σ_- (red curve) PL. We observe four main emission bands in the spectra. The one centered approximately at 640 nm (1.94 eV) is labeled LS and is attributed to emission of donor-acceptor and localized states[11,14,21]. The other 3 emissions are attributed to excitonic states of WS_2[14,19,21,35]. The higher energy emission at 591 nm (2.1 eV) is attributed to the neutral exciton (X) state. The two emissions at 598 nm (2.07 eV) and 605 nm (2.05 eV) labeled T_1 and T_2, respectively, are attributed to two negatively charged exciton states, which will be discussed in more details in the next paragraphs. Figure 1(b) also shows that the excitonic states of large-scale WS_2 are valley polarized, thus demonstrating the momentum conservation for circular polarization selection rules (depicted in Figure 1(c)) and the efficient initialization of carrier pseudospins in a given valley[2,15,36,37].

Figure 2(a) shows macro-PL spectra of our WS_2 ML under different excitation intensities measured at 532 nm. Even at very low powers, all four emissions previously identified in Figure 1(b) can be observed. As power is increased, T_1 and T_2 become more pronounced and dominate the spectra. This is evidenced in Figure 2(b), where the peak intensity for each emission is plotted as function of the excitation power (P). The solid lines represent fittings with $I_{PL} = AP^{\beta}$, where A and β are constants. We observe that X and LS emissions increase sublinearly with β values of 0.72 and 0.65, respectively. The tendency for a faster saturation of the LS band is consistent with the limited density of localized and donor-acceptor states in the material. T_1 and T_2 emissions increase faster with power. T_2 increases at a slightly faster rate (β=1.1) as compared to T_1 (β=0.93). As shown on the inset of Figure 2(a), T_2 can be observed even at the smallest power we detected the PL signal (7.95 W/cm^2), which is more than one order of magnitude lower than the power needed to observe XX emission in WS_2 MLs grown on boron nitride[38]. It is well known that the presence of boron nitride considerably suppresses laser induced doping with carriers injected from the substrate into the TMD ML[22]. As we will discuss in the next paragraphs, our samples show strong laser induced doping effects. Considering also that our samples are not defect-free and electron-doped, we believe that, at such lower powers, XX formation would not be favoured in the experiments reported in Figure 2(a). In this way, we attribute T_2 to a second negatively charged exciton emission, in agreement with other reports in the literature[11,13,39].

It is already known that different configurations of three particle complexes such as intravalley- (carriers are located within the same valley) and intervalley-(carriers are in different valleys) trions can be formed in WS_2.

In the lowest energy bright trion configuration (T_1), the excess electrons occupy the lowest energy subband in the conduction band[11]. In this case, the excess electron that constitutes the charged exciton might be in the same (singlet) or different (triplet) valley state. An energetic splitting between these two configurations (which is not resolved in our experiments), usually called trion fine structure, is determined by intervalley electron-hole exchange interaction [19,20,40]. In the highest energy trion configuration (T_2), both electrons occupy the upper conduction-band subband and, therefore, are expected to be brighter at higher excitation intensity conditions. T_2 also comprises an intravalley singlet and an intervalley triplet trions (also not resolved in our experiments). The energy separation between T_1 and T_2 observed in our experiments is 20 meV, which is also in very good agreement with literature reports[11,13]. Note that we also considered the possibility of assigning the rise of T_2 to a dark trion brightening process. However, our assignment of T_2 peak to a bright trion is supported by the fact that the energy separation between the T_1 and T_2 emissions expected for the dark trion process is $2\Delta_{SO}$[10] which, given the experimental value of 20 meV, would imply in Δ_{SO} values considerably smaller than the predicted ones[41–43].

Figure 3(a) presents macro-PL spectra (at a fixed laser power) taken with time intervals of few minutes between each measurement. We observed that, in approximately 40 minutes, X and LS emissions decrease by considerable amounts, with LS emission decreasing more than X in absolute values. T_1 also decreases at a slower rate while T_2 increases with time. The quenching of LS emission under strong laser pumping and the appearance of an emission band at the lower energy side of T_1 has already been reported in literature[21]. The quenching of LS has been interpreted as laser induced removal of surface adsorbents (associated with LS emission)[21,44]. Surface desorption may leave carriers in the system. However, laser exposure has also been demonstrated to lead to another efficient way to dope the system via carrier injection from the substrate[22]. We, therefore, attribute the increase of T_2 emission with time to an enhanced probability that electrons occupy the upper conduction subband states due to high electron doping induced by laser irradiation[22,45]. This enhancement of T_2 emission (in comparison to X and T_1) with photo doping is consistent with the results obtained by electron injection in gated devices[11]. In this way, we use laser irradiation as a contactless approach to induce changes in the spectrum of WS_2 and identify T_2 as a trionic state. This is further confirmed in Figure 3(b), where the intensities of X, T_1, and T_2 as function of time are normalized by the LS emission since this emission is associated with surface desorption and, therefore, also responsible for doping the system. We observe that, relative to LS emission, T_1 and T_2 emissions increase at very similar rates when electrons are added to the system. This behavior further

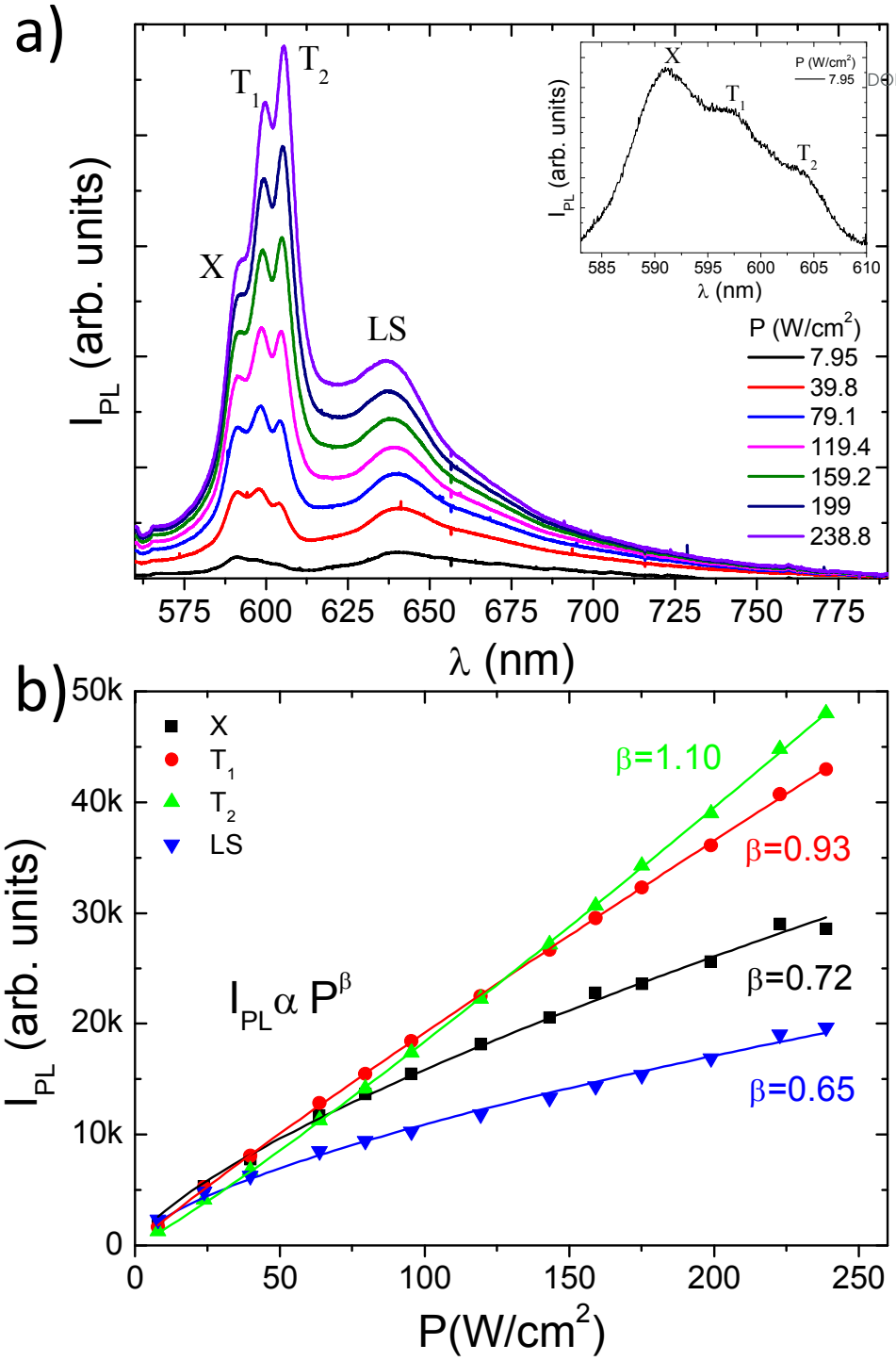

FIG. 2: (a) Macro-PL measured at 12 K for WS_2 monolayer as function of excitation power. Inset: main excitonic emission band measured at 7.95 W/cm^2.(b) PL intensity as a function of excitation power for X, T_1, and T_2, and LS emission. Solid lines correspond to fits with $I_{PL} = AP^{\beta}$, where A and β are constants. The values of β obtained from each fit are displayed for each emission.

corroborates our attribution of T_2 to a trion state rather than a XX one. As also seen in Figure 3(b), X emission is more independent of the changes in LS. The absolute decrease in X intensity is attributed to the formation of charged complexes as the system is further doped with increase of time.

In order to obtain more information about the doping dynamics and emission stability in our sample in a microscopic level, we performed μ-PL measurements under different excitation power conditions. Figure 4 presents a μ-PL experiment performed at 10 K with a laser spot diameter of approximately 5 μm at 532 nm. Figure 4(a) presents a sequence of measurements where laser power is increased (blue curves) and then lowered (red curves). The first spectrum (at 50.9 W/cm^2) shows a pronounced LS band and the excitonic features of X and T_1 emissions. As power is raised T_2 emission becomes more pronounced and the excitonic emissions dominate the spectrum in comparison to LS emission (1528 W/cm^2). As power is lowered, however, the spectra do not resume back to their initial characteristics. When we compare the spectra measured at 50.9 W/cm^2, the X emission is similar in the blue and red curves, but LS emission is weaker and T_2 maintains its dominant behaviour in the red spectrum. This irreversible behaviour of LS band is consistent with the already mentioned surface desorption induced by laser power[21]. The desorption seems to leave electrons in the system which contribute to the preservation of the T_2 emission even at very low laser powers. Moreover, the fact that the X emission changes very slightly while T_2 changes drastically when power is lowered also corroborates our attribution of T_2 to a trion state. If T_2 was due to a biexciton recombination, which depends strongly on the exciton density, T_2 should more or less follow the X emission behavior.

When the power density is high, however, other emissions might also contribute to the intensity of T_2 peak. This is shown in Figure 4(b), where the logarithm of the peak intensity of this emission is plotted as a function of the logarithm of the excitation power. Blue dots represent power increase and red dots represent power decrease. It is observed that the behaviour is definitely non-linear and it is not possible to fit the data (in the same way we performed in macro-PL experiments) with a dependence such like $I_{PL} = AP^{\beta}$ with a single value for β. At very high carrier densities, other excitonic peaks like bound XX[12,14,15] and/or charged XX[46] (which are observed/expected to be observed in the same energy range) may also be contributing to the overall T_2 intensity.

Another feature observed in the spectra shown in Figure 4(a) (highlighted by dashed square boxes) is the random appearance of extra emission lines in the lower energy side of T_2. For example, the features highlighted at 1528 W/cm^2 laser power have not been detected in the previous measurement at 1019 W/cm^2 (blue spectrum) and are hardly seen again in the sequence at 1019 W/cm^2 (red spectrum). Other examples can be seen at 254.7

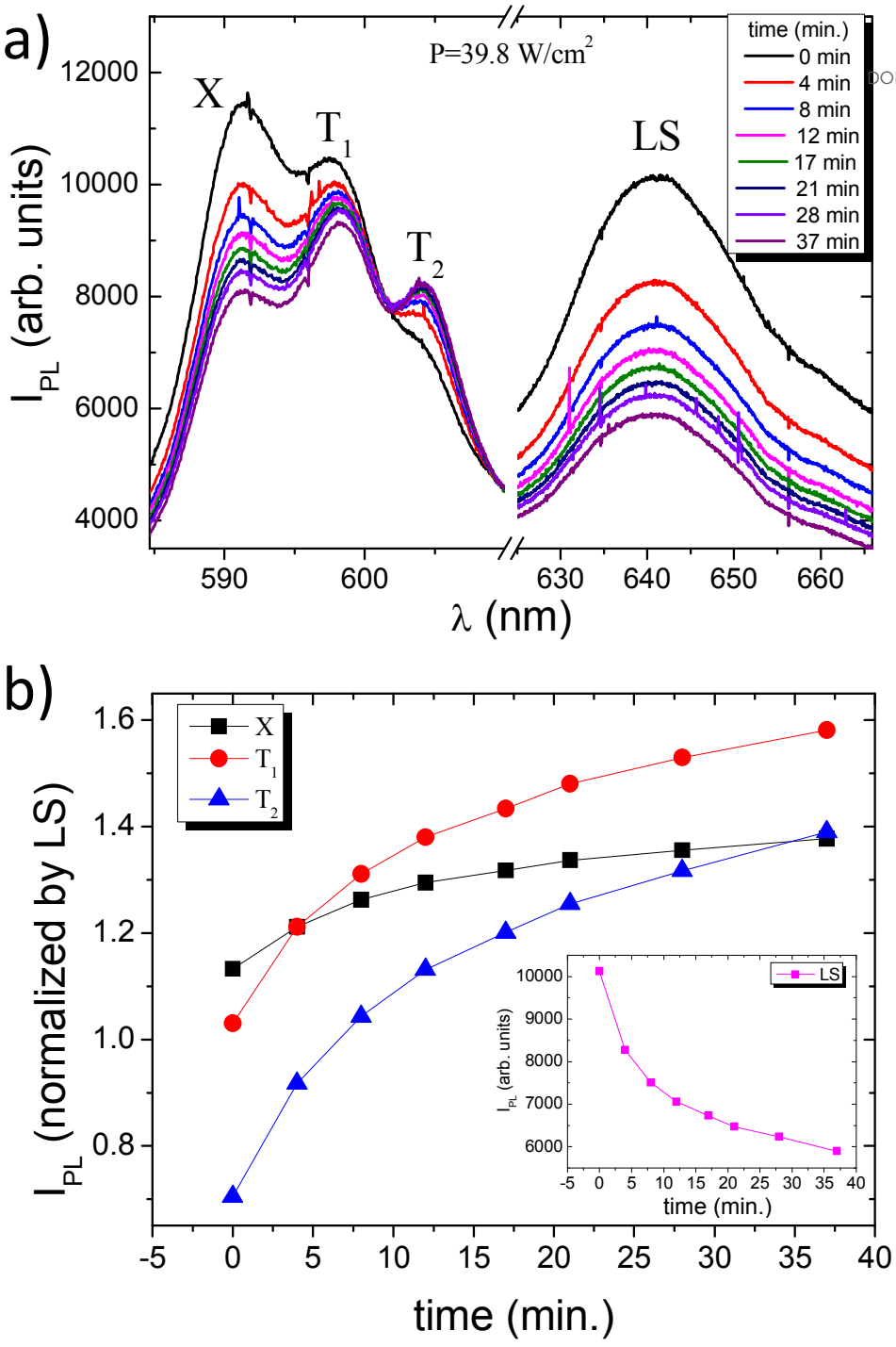

FIG. 3: (a) PL spectra at 12 K and fixed excitation power for different times after the first measured spectrum (black curve). (b) PL intensity of X, T_1, and T_2 emissions normalized by the LS emission intensity (shown on the inset) for different times after first measured spectrum.

and 127.3 W/cm^2 spectra (red curves), where the highlighted features appear in the lowering of the power but were not there when power was raised. These unstable peaks appear in an energy region which is usually expected to present recombination of impurity bound exciton states[11,14]. The high carrier density induced in μ-PL excitation seems to be more efficient in activating this kind of recombination, which is a process possibly linked to the surface desorption already discussed.

Figure 5 presents time stability of the μ-PL emission of our sample when the laser spot is further reduced to 2 μm. As we observe in Figure 5(a), when the probing spot size is reduced it is easier to identify the contribution of T_2 and bound states (labeled X_B). Figure 5(b) shows how the μ-PL spectrum changes with time in an interval of 20 minutes under 318 W/cm^2 excitation at 488 nm. A few minutes after the first spectrum is acquired, we observe that X and LS emissions almost vanish in intensity. T_1 also decreases initially, but seems to keep its intensity as time passes. T_2, on the other hand, gains intensity with time. This is consistent with macro-PL results shown in Figure 3 and illustrates once more the role of carrier doping induced by laser excitation on the optical emission of neutral and charged excitons. It is interesting to note the behaviour of X_B emission in Figure 5(b). The sharp lines which characterize this emission (with linewidths which can reach 2 meV) are not stable, with variations in intensity and spectral position. This is an indication that the carrier trap/release process by impurity states happens in a time scale of minutes which is the same scale that T_2 gains intensity with time. The same behaviour is observed when the measurement is performed at different positions on the sample surface. This is presented in Figures 5(c) and (d). The main difference here is that, due to the higher excitation power (637 W/cm^2), X and LS emissions seem to be almost immediately quenched due to the accelerated doping process.

Figure 6 shows how the emission of our WS_2 monolayer changes in time when it is submitted to extreme laser powers (laser spot of 2 μm at 488 nm). Each column of viewgraphs represents measurements at different temperatures (4, 50, and 160 K). Horizontally, power is changed. In this way, for each temperature, μ-PL evolution in time is tracked in a sequence of four measurements. First, immediately after the sample is subjected to a laser excitation of 637 W/cm^2, the PL emission is tracked for 20 minutes. Then the power is increased to 31.8 kW/cm^2 and the measurement is performed once more (for 60 seconds). Subsequently, the laser incidence is maintained on the sample and, after 10 minutes, the last experiment is repeated. Finally, the power is lowered again to 637 W/cm^2 and the PL is measured once more during 20 minutes. At 4 K and 637 W/cm^2(first measurement), the behaviour is exactly the same as illustrated in Figures 5(c) and (d). When the power is

View Article Online
DOI: 10.1039/C8NR00719E

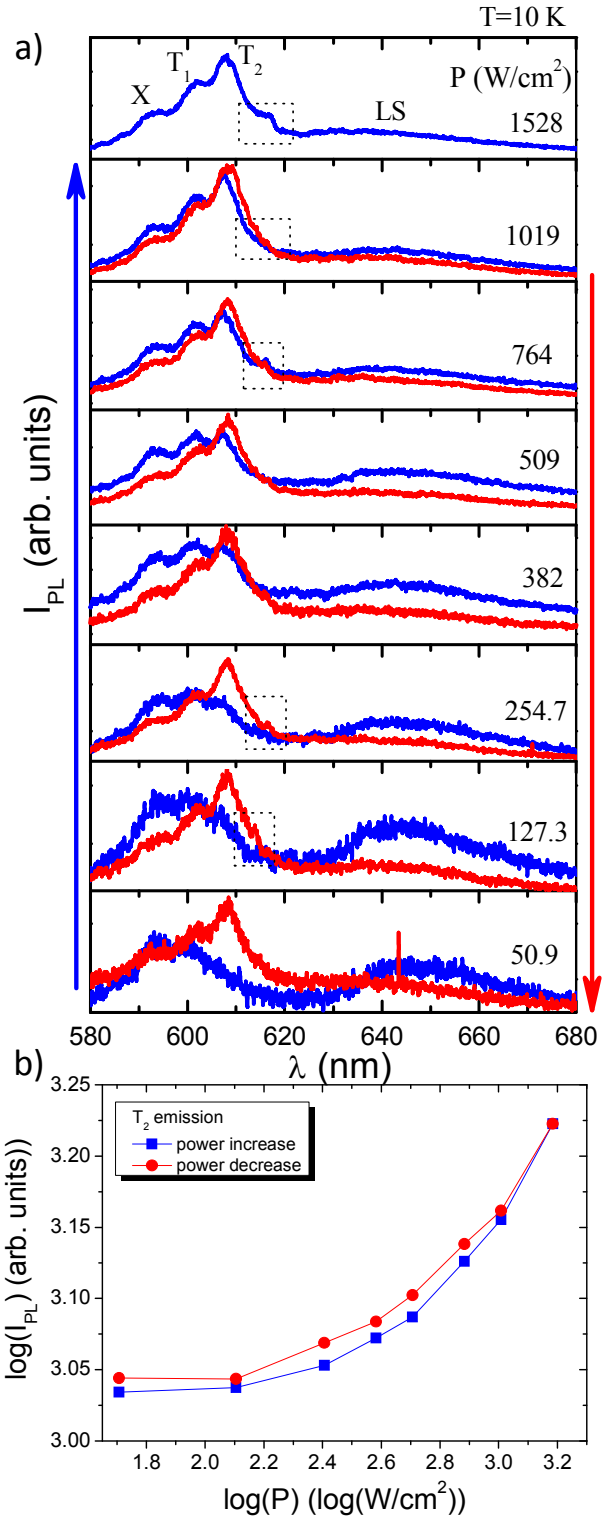

FIG. 4: (a) From bottom to top (blue curves): PL spectra of WS_2 monolayer as excitation power is increased from 50.9 to 1528 W/cm^2. From top to bottom (red curves): PL spectra as excitation power is decreased back to 50.9 W/cm^2. Dashed squares indicate small changes in the spectra which do not behave in a consistent way as power is increased or decreased. (b) Integrated PL intensity versus excitation power extracted from (a).

View Article Online
DOI: 10.1039/C8NR00719E

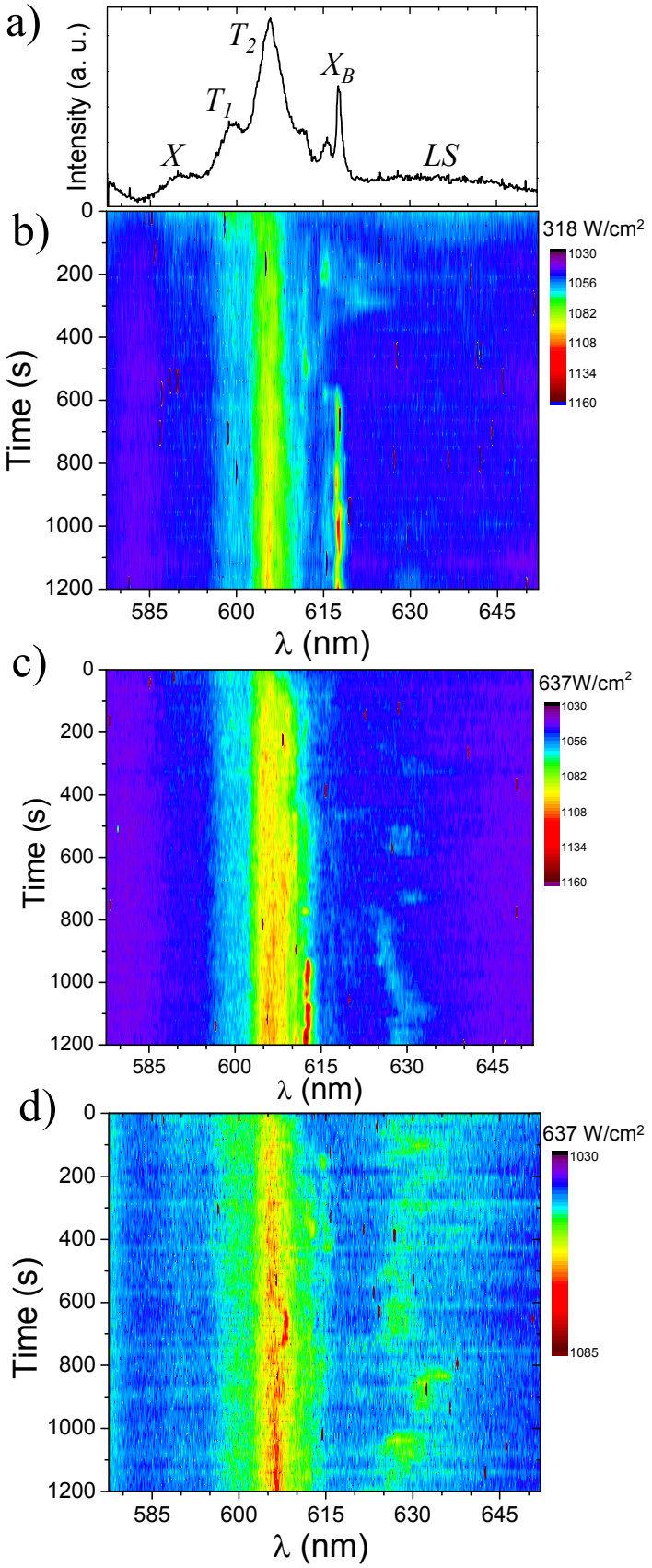

FIG. 5: (a) μ-PL spectra shown in (b) integrated in time. (b), (c), and (d) Time variation of μ-PL spectra of WS_2 monolayer in the lower excitation power regime for 3 different position on the sample surface.

increased to 31.8 kW/cm^2, a strong redshift of the emission band is observed. Nevertheless, the emission is still unstable and seems to increase in intensity as time passes. This is an indication that electron doping is still taking place in the system. After 10 minutes of exposure under strong pumping conditions, the emission is slightly more redshifted and has gained intensity in comparison to the previous measurement. Instability still takes place, as we can observe the appearance/disappearance of sharp lines with time in the lower energy side of T_2 band. As power is reduced back to 637 W/cm^2 (lower viewgraph in the first column), the emission does not blueshift back and the intensity is higher than in the first measurement at the same power. Figure 7(a) summarizes these experiments by showing the time integrated μ-PL for each view graph of the first column of Figure 6. By reducing the power after strong pumping conditions, we observe that the neutral exciton emission is quenched (blue curve), while the spectrum is dominated by T_2 and X_B emissions which are strongly favoured after laser doping. The process is, therefore, irreversible and the spectrum maintains its redshift with respect to the initial measurement.

Figure 6 also shows how the emission instability varies with temperature. At 50 K and low power, μ-PL spectrum is slightly broader, but it is still possible to see the enhancement of T_2 emission with time and the appearance/disappearance of sharp peaks in the X_B emission region. As power is increased, the PL spectrum gains intensity with exposure time. As power is lowered back, the redshift is also not reversed and the intensity is higher than at the beginning of the experiment, in a similar way to what happens at 4 K. A different behaviour is observed at 160 K. At this temperature, under low power, the PL spectra exhibit broad emission and the whole spectrum moves to the lower energy as time passes. Besides, the X_B related sharp peaks are no more observed. As power increases the redshift is enhanced. As power is lowered again, the spectrum is dominated by a broad emission which superimposes trions (PL measurements as function of temperature, not shown, demonstrate that at this temperature T_1 and T_2 emissions tend to merge and have comparable intensities) and X_B emission bands. This is shown in Figure 7(b) (blue spectrum). However, the lower viewgraph of the third column of Figure 6 indicates that, when power is lowered back to its initial value at 160 K, a slight blueshift of the emission starts to happen in a very slow time scale. This indicates that elevated temperatures are possibly an important ingredient to revert laser induced doping in these TMD monolayers. However, the time scale seems to be slow enough even at room temperature[23]. The overall behaviour of our sample clearly shows that doping/undoping of the WS_2 monolayer is a very slow process which depends on time and pumping laser power. Moreover, we show that the effect is present even at relatively elevated temperatures. These are very important issues which can affect the

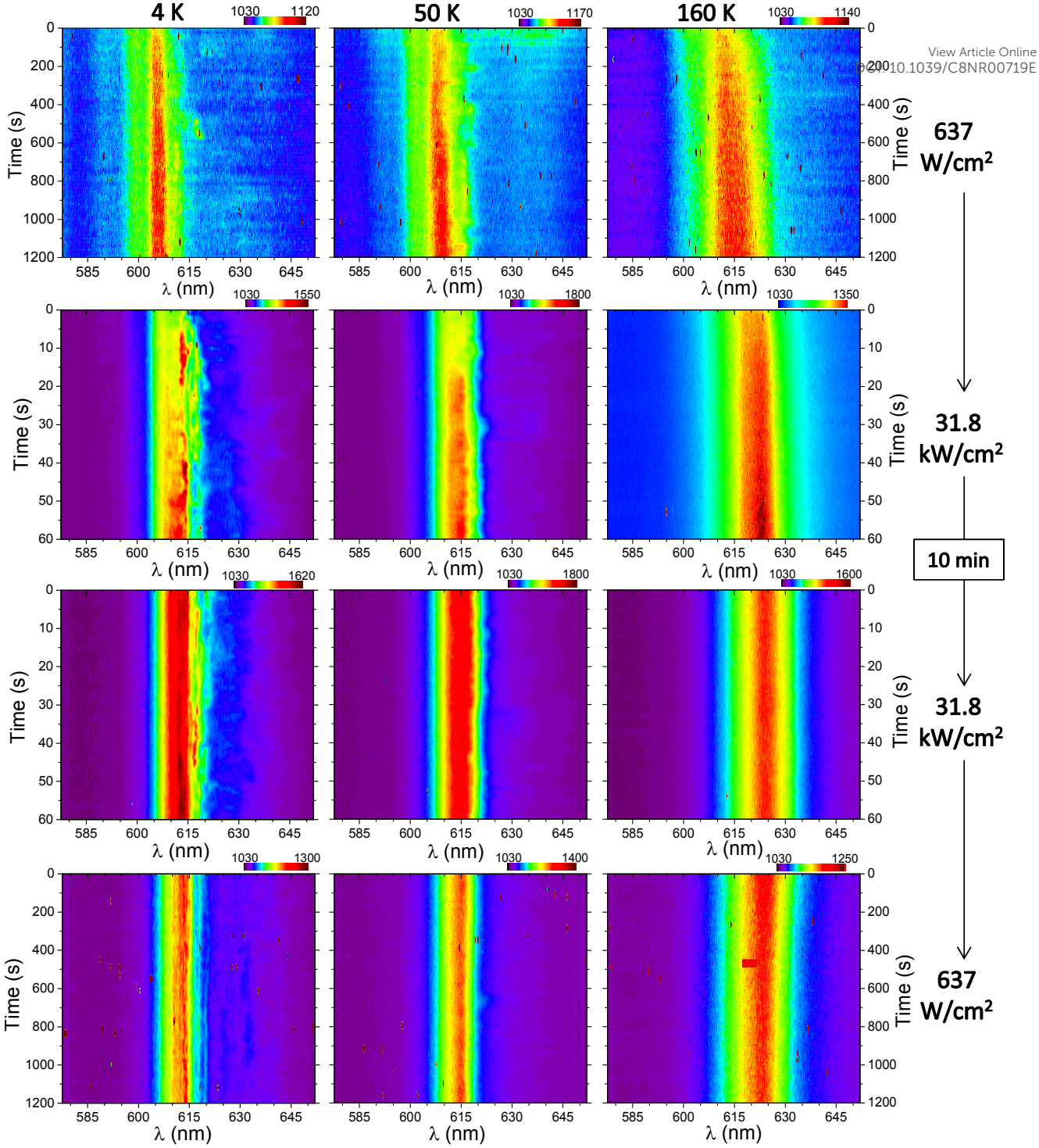

FIG. 6: Color code map showing the variation of μ-PL of WS_2 monolayer in time. First row: excitation power set at 637 W/cm^2. Second row: power is increased to 31.8 kW/cm^2. Third row: waited for 10 minutes under 31.8 kW/cm^2 and repeated previous measurement. Fourth row: power is decreased back to 637 W/cm^2. The same procedure is repeated for different temperatures [4K (left column), 50K (middle column), and 160K (right column)].

performance of future optoelectronic devices based on this type of TMD[6].

View Article Online
DOI: 10.1039/C8NR00719E

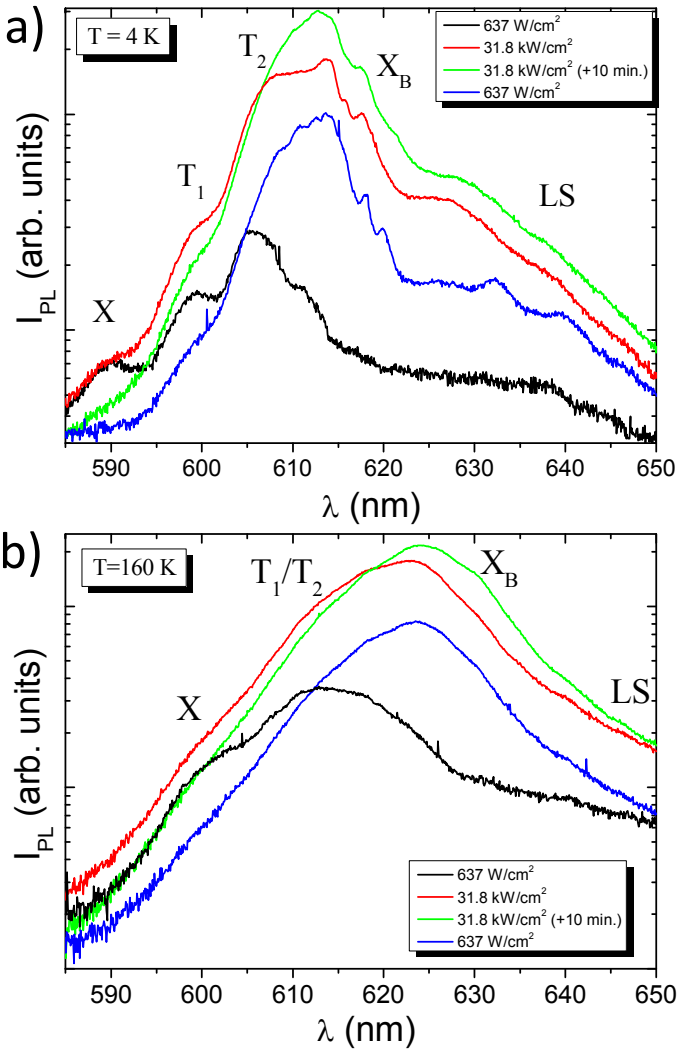

FIG. 7: (a) Time integrated μ-PL spectra for the four viewgraphs shown in the first column of Figure 6 (4 K). (b) Time integrated μ-PL spectra for the four viewgraphs shown in the last column of Figure 6 (160 K).

III. CONCLUSIONS

We have investigated the nature of optical emission and laser irradiation effects on the optical properties of large-scale Van der Waals epitaxially grown WS_2 monolayers. We showed that laser irradiation results in dramatic changes in the relative intensity of the individual exciton emission lines. As power or laser exposure time are increased, we show that monolayer doping builds up on a time scale of minutes and can be detected by the pronounced increase in the emission intensities of the two trion emissions T_1 and T_2. The enhancement of

trionic emissions, particularly T_2, is demonstrated to be due to carrier injection from substrate and desorption of surface molecules which contribute to the doping process. Reduction of the probing area shows that local carrier recombination dynamics under continuous doping conditions is complex. In particular, bound electron states which present sharp emission lines show considerable intensity instability with time. Under strong laser pumping conditions, the spectra of exposed areas are irreversibly changed, presenting large redshifts due to the dominance of the spectra by trions, bound exciton states, and possibly XX complexes. Temperature increase may contribute to reverting the process, but our experiments indicate that the time scales are still long. Our results can contribute to a better understanding of the optical properties and photo-induced doping process mechanism in laser-scale VdWE WS_2 monolayers, which is of great interest for future nanodevices employing this material system.

IV. EXPERIMENTAL METHODS

We investigated large-scale (10 mm by 10 mm) WS_2 MLs grown on 300 nm thick thermal oxide (SiO_2) on silicon substrates by Van der Waals epitaxy (VdWE) process. VdWE can provide the vapour phase epitaxy of these layered TMDs on the substrates even with mismatched lattice constants[34]. Here, for the first time VdWE technique has been successfully developed to fabricate large-scale ML WS_2 on quartz and SiO_2/Si wafers. Different from typical CVD growth which has been demonstrated to provide large-scale ML films formed by the growth and merging of individual TMD flakes[47,48], VdWE technique allows very fast growth (typically 5 minutes) of continuous and homogeneous WS_2 ML films (typical sizes are 25 mm by 25 mm with in-house built system at the University of Southampton) . VdWE-grown ML characteristics can be found in the Supporting Information section. Figure S.1 shows the spatial homogeneity of a ML of WS_2 grown on 300 nm SiO_2/Si and quartz substrates . The spatial and structural homogeneity of our WS_2 ML films are demonstrated by using Raman (see Figure S.2) and PL (see Figure S.3) spectroscopy measurements taken at room temperature

In the preparation of our VdWE-grown WS_2 MLs samples, WCl_6 (99.9% pure from Sigma Aldrich) was used as the precursor, kept in a bubbler at room temperature and delivered to VdWE quartz tube reactor (with 50 mm diameter and 1000 mm length) to react with H_2S gas (99.9% pure from BOC) to form WS_2 epitaxially on SiO_2/Si substrates at temperatures in the range of 700-1000°C. WCl_6 vapors were delivered with argon gas (99.999% pure from BOC) through a mass flow controller (MFC) and the H_2S gas was delivered through another MFC. The flow rates of argon and H_2S gases were in the ranges of 50 - 300 mL/min. These Van der Waals epitaxially

grown WS_2 MLs on SiO_2/Si substrates are illustrated in Figure 1(a). Hall measurements show that samples are n-type.

View Article Online
DOI: 10.1039/C8NR00719E

Macro-PL measurements were performed using a closed-cycle refrigerator cryostat. μ-PL measurements were carried out in vacuum with He cryostat equipped with three-axis stepper motors to control the sample position. The samples were excited using 488 and 532 nm solid state laser sources. The laser spot diameter on the sample for Macro-PL measurements is approximately 400 μm. For μ-PL spot sizes of 5 and 2 μm were employed. In all experiments, detection was performed with 0.5 m spectrometers coupled with Si CCD detectors.

V. CONFLICTS OF INTEREST

There are no conflicts to declare.

VI. ACKNOWLEDGEMENTS

The authors acknowledge V. I. Falko for the discussions and A. G. Rodrigues for Raman measurements. The authors also acknowledge the financial supports from the Brazilian agencies (Fundação de Amparo a Pesquisa do Estado de São Paulo (FAPESP grants 2012/11382-9, 2016/10668-7, 2016/16365-6, and 2014/50513-7) and Conselho Nacional de Desenvolvimento Científico e Tecnológico (CNPq) (grant 305769/2015-4). and the UK Engineering and Physical Sciences Research Council. This work was funded in part through the Future Photonics Manufacturing Hub at the University of Southampton (EPSRC EP/N00762X/1). The data that support the findings of this study are available from the corresponding authors upon reasonable request.

* Electronic address: yara.ufscar@gmail.com

† Electronic address: cch@orc.soton.ac.uk

[1] Q. H. Wang, K. K. Zadeh, A. Kis, J. N. Coleman, and M. S. Strano, Nat. Nanotech **7**, 699 (2012).

[2] X. Xu, W. Zao, D. Xiao, and T. F. Heinz, Nature Phys. **10**, 343 (2014).

[3] H. Zeng and X. Cui, Chem. Soc. Rev. **44**, 2629 (2015).

[4] Y. Ye, Z. J. Wong, X. Lu, X. Ni, H. Zhu, X. Chen, Y. Wang, and X. Zhang, Nat. Photon **9**, 733 (2015).

[5] A. V. Kolobov and J. Tominaga, *Two-Dimensional Transition-Metal Dichalcogenides* (Springer, 2016).

[6] K. F. Mak and J. Shan, Nature Photon. **10**, 216 (2016).

View Article Online
DOI: 10.1039/C8NR00719E

[7] L. Klopotowski, C. Backes, A. A. Mitioglu, V. Vega-Mayoral, D. Hanlon, J. N. Coleman, V. Y. Ivanov, D. K. Maude, and P. Plochocka, Nanotechnology **27**, 424701 (2016).

[8] M. Koperski, M. R. Molas, A. Arora, K. Nogajewski, A. O. Slobodeniuk, C. Faugeras, and M. Potemski, Nanophotonics **6**, 1289 (2017).

[9] F. Wu, F. Qu, and A. H. MacDonald, Phys. Rev. B **91**, 075310 (2015).

[10] M. Danovich, v. Zolyomi, and V. I. Falko, Sci. Rep **7**, 45998 (2017).

[11] M. R. Molas, K. Nogajewski, A. O. Slobodeniuk, J. Binder, M. Bartos, and M. Potemski, Nanoscale (2017).

[12] E. Mostaani, M. Szyniszewski, C. H. Price, R. Maezono, M. Danovich, R. J. Hunt, N. D. Drummond, and V. I. Falko, Phys. Rev. B **96**, 075431 (2017).

[13] J. J. an J. K. Girzycka, P. Kapuscinski, Y. S. Huang, A. Wojs, and L. Bryja, Nanotechnology **28**, 395702 (2017).

[14] G. Plechinger, P. Nagler, J. Kraus, N. Paradiso, C. Strunk, C. Schueller, and T. Korn, Phys. Status Solidi **8**, 457 (2015).

[15] Y. You, X. X. Zhang, T. C. Berkelbach, M. S. Hyberstsen, D. R. Reichman, and T. F. Heinz, Nature Phys. **11**, 477 (2015).

[16] J. Shang, X. Shen, C. Cong, N. Peimyoo, B. Cao, M. Eginligil, and T. Yu, ACS Nano **9**, 647 (2015).

[17] Z. He, W. Xu, Y. Zhou, X. Wang, Y. Sheng, Y. Rong, S. Guo, J. Zhang, J. M. Smith, and J. H. Warner, ACS Nano **10**, 2176 (2016).

[18] I. Paradisanos, S. Germanis, N. T. Pelekanos, C. Fotakis, E. Kymakis, G. Kioseoglou, and E. Stratakis, Appl. Phys. Lett. **110**, 193102 (2017).

[19] G. Plechinger, P. Nagler, A. Arora, R. Schmidt, A. Chernikov, A. G. del Aguila, P. C. M. Christianen, R. Bratschitsch, C. Schuller, and T. Korn, Nat. Commun. **7**, 12715 (2016).

[20] A. Singh, K. Tran, M. Kolarczik, J. Seifert, Y. Wang, K. Hao, D. Pleskot, N. M. Gabor, S. Helmrich, N. Owschimikov, et al., Phys. Rev. Lett. **117**, 257402 (2016).

[21] Z. He, X. Wang, W. Xu, Y. Zhou, Y. Sheng, Y. Rong, J. M. Smith, and J. H. Warner, ACS Nano **10**, 5847 (2016).

[22] F. Cadiz, C. Robert, G. Wang, W. Kong, X. Fan, M. Blei, D. Lagarde, M. Gay, M. Manca, T. Taniguchi, et al., 2D Materials **3**, 045008 (2016).

[23] Y. Lee, S. J. Yun, M. S. Kim, G. H. Han, A. K. Sood, and J. Kim, Nanoscale **9**, 2272 (2017).

[24] S. Dufferwiel, S. Schwarz, F. Withers, A. A. P. Trichet, F. Li, M. Sich, O. D. Pozo-Zamudio, C. Clark, A. Nalitov, D. D. Solnyshkov, et al., Nat. Commun. **6**, 8579 (2015).

[25] Y. M. He, G. Clark, J. R. Schaibley, Y. He, M. C. Chen, Y. J. Wei, X. D. Ding, Q. Zhang, W. Yao, X. Xu, et al., Nat. Nanotech. **10**, 497 (2015).

[26] A. Srivastava, M. Sidler, A. V. Allain, D. S. Lembke, A. Kis, and A. Imamoglu, Nanotechnology **10**, 491 (2015).

View Article Online
DOI: 10.1039/C8NR00719E

[27] M. Koperski, K. Nogajewski, A. Arora, V. Cherkez, P. Mallet, J.-Y. Veuillen, J. Marcus, P. Kossacki, and M. Potemski, Nat. Nanotech. **10**, 503 (2015).

[28] C. Palacios-Berraquero, D. M. Kara, A. R. P. Montblanch, M. Barbone, P. Latawiec, D. Yoon, A. K. Ott., M. Loncar, A. C. Ferrari, and M. Atature, Nat. Commun. **8**, 15093 (2017).

[29] C. Chakraborty, L. Kinnischtzke, K. M. Goodfellow, R. Beams, and A. N. Vamivakas, Nat. Nanotech. **10**, 507 (2015).

[30] G. Clark, J. R. Schaibley, J. Ross, T. Taniguchi, K. Watanabe, J. R. Hendrickson, S. Mou, W. Yao, and X. Xu, RSC Adv **6**, 27677 (2016).

[31] Y. He, O. Iff, N. Lundt, V. Baumann, M. Davanco, K. Srinivasan, and S. H. andC. Schneider, Nat. Commun. **7**, 13409 (2016).

[32] S. Schwarz, A. Kozikov, F. Withers, J. K. Maguire, A. P. Foster, S. Dufferwiel, L. Hague, M. N. Makhonin, L. R. Wilson, and A. K. Geim, 2D Materials **3**, 025038 (2016).

[33] T. Kato and T. Kaneko, ACS Nano **8**, 12777 (2014).

[34] A. Koma, J. Crys. Growth **201**, 236 (1999).

[35] W. Yang, J. Shang, J. Wang, X. Shen, B. Cao, N. Peimyoo, C. Zou, Y. Chen, Y. Wang, C. Cong, et al., Nano Lett. **16**, 1560 (2016).

[36] D. Xiao, G. B. Liu, W. Feng, X. Xu, and W. Yao, Phys. Rev. Lett. **108**, 196802 (2012).

[37] A. M. Jones, H. Yu, N. M. G. S. Wu, G. Aivazian, J. S. Ross, B. Zhao, J. Yan, D. G. Mandrus, D. Xiao, W. Yao, et al., Nat. Nanotech. **8**, 634 (2013).

[38] M. Okada, Y. Miyauchi, K. Matsuda, T. Taniguchi, K. Watanabe, H. Shinohara, and R. Kitaura, Sci. Rep. **7**, 322 (2017).

[39] A. Boulesbaa, B. Huang, K. Wang, M. W. Lin, M. M. Samani, C. Rouleau, K. Xiao, M. Yoon, B. Sumpter, A. Puretzky, et al., Phys. Rev. B **92**, 115443 (2015).

[40] G. Plechinger, P. Nagler, A. Arora, M. B. A. G. del Aguila, T. Frank, P. Steinleitner, M. Gmitra, J. Fabian, P. C. M. Christianen, R. Bratschitsch, et al., Nano Lett. **16**, 7899 (2016).

[41] G. B. Liu, W. Y. Shan, Y. Yao, W. Yao, and D. Xiao, Phys. Rev. B **88**, 085433 (2013).

[42] K. Kosmider, J. W. Gonzalez, and J. Fernandez-Rossier, Phys. Rev. B **88**, 245436 (2013).

[43] A. Kormanyos, G. Burkard, M. Gmitra, J. Fabian, V. Zolyomi, N. D. Drummond, and v. Falko, 2D Materials **2**, 022001 (2015).

[44] K. D. Shiang, Surf. Sci. **292**, 145 (1993).

[45] X. H. Wang, J. Q. Ning, Z. C. Su, C. C. Zheng, B. R. Zhu, L. Xie, H. S. Wua, and S. J. Xu, RSC Adv **6**, 27677 (2016).

[46] K. Hao, J. F. Specht, P. Nagler, L. Xu, K. Tran, A. Singh, C. K. Dass, C. Schueller, T. Korn, M. Richter, et al., Nature Comm. **8**, 15552 (2017).

[47] Y. Zhang, Y. Zhang, Q. Ji, J. Ju, H. Yuan, J. Shi, T. Gao, D. Ma, M. Liu, Y. Chen, et al., ACS Nano **7**, 8963 (2013).

[48] K. Kang, S. Xie, L. Huang, Y. Han, P. Y. Huang, K. F. Mak, C. J. Kim, D. Muller, and J. Park, Nature **520**, 656 (2015).

View Article Online
DOI: 10.1039/C8NR00719E